OCT4 controls mitotic stability and inactivates the RB tumor suppressor pathway to enhance ovarian cancer aggressiveness

E Comisso[1,2], M Scarola[1,6], M Rosso[1,3,6], S Piazza[1,4], S Marzinotto[5], Y Ciani[1], M Orsaria[5], L Mariuzzi[5], C Schneider[1,2], S Schoeftner[1,3] and R Benetti[1,2]

OCT4 (Octamer-binding transcription factor 4) is essential for embryonic stem cell self-renewal. Here we show that OCT4 increases the aggressiveness of high-grade serous ovarian cancer (HG-SOC) by inactivating the Retinoblastoma tumor suppressor pathway and enhancing mitotic stability in cancer cells. OCT4 drives the expression of Nuclear Inhibitor of Protein Phosphatase type 1 (NIPP1) and Cyclin F (CCNF) that together inhibit Protein Phosphatase 1 (PP1). This results in pRB hyper-phosphorylation, accelerated cell proliferation and increased *in vitro* tumorigenicity of ovarian cancer cells. In parallel, OCT4 and NIPP1/CCNF drive the expression of the central Chromosomal Passenger Complex (CPC) components, Borealin, Survivin and the mitotic kinase Aurora B, promoting the clustering of supernumerary centrosomes to increase mitotic stability. Loss of *OCT4* or *NIPP1/CCNF* results in severe mitotic defects, multipolar spindles and supernumerary centrosomes, finally leading to the induction of apoptosis. These phenotypes were recapitulated in different cancer models indicating general relevance for human cancer. Importantly, activation of these parallel pathways leads to dramatically reduced overall survival of HG-SOC patients. Altogether, our data highlights an unprecedented role for OCT4 as central regulator of mitotic fidelity and RB tumor suppressor pathway activity. Disrupting this pathway represents a promising strategy to target an aggressive subpopulation of HG-SOC cells.

INTRODUCTION

OCT4 is a key transcription factor that regulates mammalian embryonic pre-implantation development and is fundamental for pluripotency and self-renewal of embryonic stem cells (ESCs).[1] Importantly, OCT4 has also been linked to cancer formation in mouse and human. Elevated OCT4 expression increased teratoma formation potential of mESCs and transgenic expression of OCT4 caused the development of various types of aggressive epithelial cancer.[2,3] Remarkably, OCT4 expressing cells isolated from spontaneously formed tumors of p53-deficient mice showed self-renewal features and supported tumor engraftment and metastasis.[4] This suggests that OCT4 supports tumor initiation and invasiveness. In human cancer OCT4 expression was detected in various types of malignant neoplasms and increased expression levels correlate with advanced tumor grade, metastasis formation and reduced survival rates, underlining the clinical relevance of OCT4.[5–7] In line with data from mouse cancer models, OCT4 expression was identified as a common feature of human cancer stem cell-like cells purified from several types of cancer, is associated with tumor-initiation potential, mediates chemoresistance, protects from apoptosis and has an impact on epithelial to mesenchymal transition.[8–16] To date the role of OCT4 in epithelial ovarian cancer (EOC) has been sparsely addressed. OCT4 expression is linked with poor cancer differentiation status, increases from normal surface or fallopian tube epithelium to benign/borderline tumors to high-grade serous ovarian carcinomas and correlates with disease progression.[17] Cell clones established from ascites of a patient with advanced ovarian cancer showed high OCT4 expression and tumor-initiation potential in xenografting experiments.[18] Importantly, cancer stem cell-like side populations derived from patients with early recurrence display increased expression of OCT4 and other stemness markers.[19,20] Although these results indicate a clinical relevance for OCT4 in EOC, OCT4 dependent pathways that promote the aggressiveness of epithelial ovarian cancer are largely unknown. Using mouse embryonic stem cells (mESCs), we recently demonstrated that OCT4 does not only ensure mESCs pluripotency but also mediates the enzymatic inactivation of the Retinoblastoma pathway.[21] In particular, OCT4 drives the expression of Nuclear Inhibitor of Protein Phosphatase 1 (NIPP1) and Cyclin F (CCNF), both inhibitors of Protein Phosphatase 1 (PP1). This pathway prevents PP1 dependent de-phosphorylation of Retinoblastoma protein 1 (pRB) mediating rapid mESCs proliferation.[21] In this study, we aimed to identify clinically relevant pathways that are regulated by OCT4 in high-grade serous ovarian cancer (HG-SOC). We show that the OCT4-NIPP1/CCNF axis mediates the enzymatic inactivation of pRB in HG-SOC cells to drive tumor cell proliferation. Past studies show that the enzymatic inactivation of pRB is coupled with mitotic instability.[22–26] Importantly, here we show that OCT4, NIPP1 and CCNF have an important role in enhancing the expression of Chromosomal Passenger Complex (CPC) components Aurora B, Survivin and Borealin. This results in improved Aurora B and CPC function, thereby ensuring mitotic stability. We thus

[1]Cancer Epigenetic Group, Laboratorio Nazionale Consorzio Interuniversitario Biotecnologie (LNCIB), Area Science Park, Trieste, Italy; [2]Department of Medical and Biological Sciences, University of Udine; Udine, Italy; [3]Department for Life Sciences, University of Trieste, Trieste, Italy; [4]Centre for Integrative Biology, University of Trento (CIBIO), Trento, Italy and [5]Department of Medical and Biological Science, Institute of Anatomic Pathology, University Hospital of Udine, Udine, Italy. Correspondence: Dr R Benetti, Cancer Epigenetic Group, Laboratorio Nazionale Consorzio Interuniversitario Biotecnologie (LNCIB), Area Science Park - Palazzina F3, Padriciano 99, Trieste 34149, Italy or S Schoeftner, LNCIB, Genomic Instability Group, Area Science Park, Padriciano 99, Trieste 34149, Italy.
E-mail: roberta.benetti@lncib.it or stefan.schoeftner@lncib.it

[6]These authors contributed equally to this work.

Accepted 11 January 2017

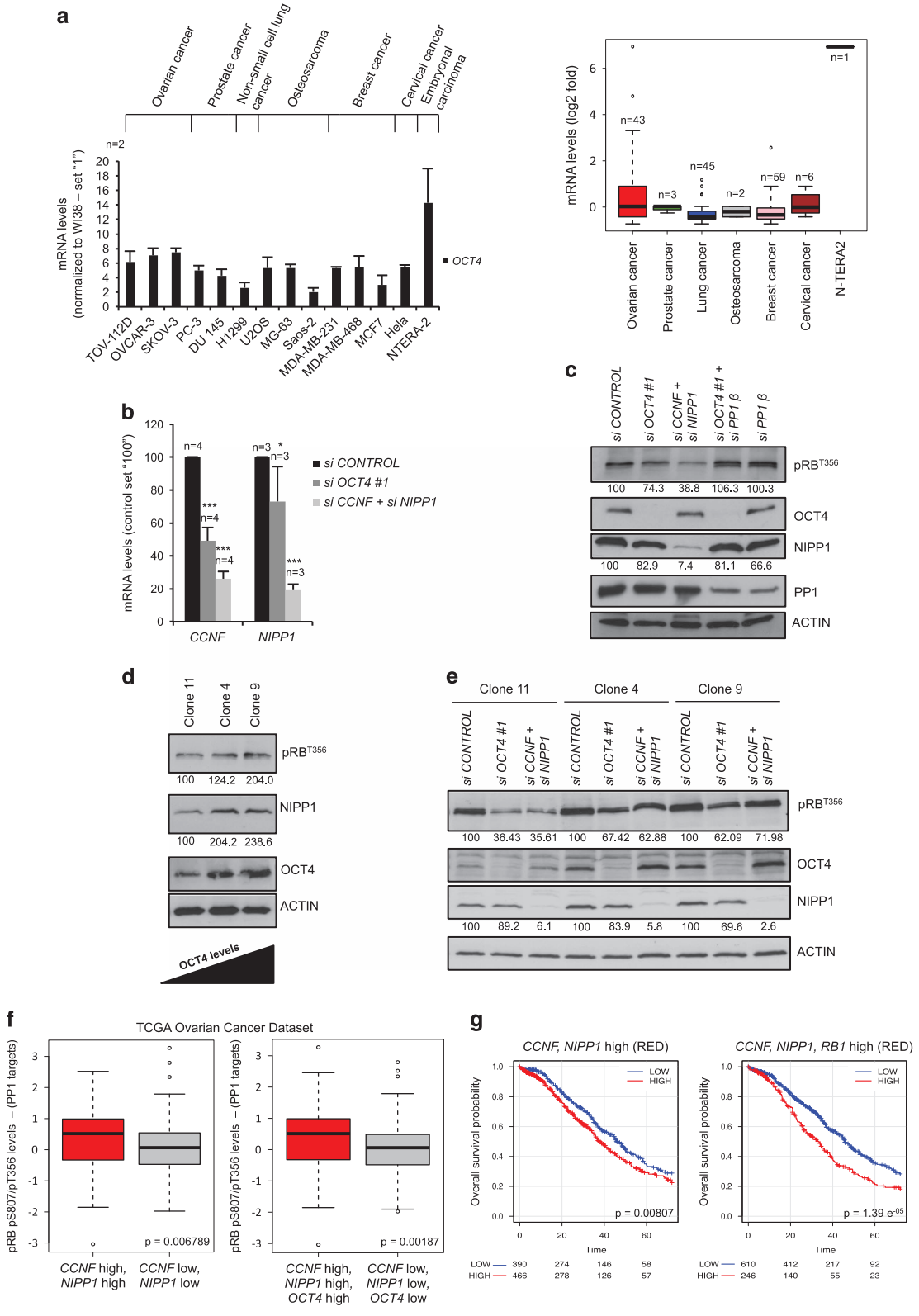

conclude that OCT4 has a central role in suppressing genomic instability resulting from RB tumor suppressor pathway inactivation in HG-SOC cells. Data from HG-SOC cancer specimen support *in vitro* data and show that elevated OCT4-NIPP1/CCNF-CPC expression defines a highly aggressive subtype of human HG-SOC.

RESULTS

The OCT4-NIPP1/CCNF-PP1 axis mediates pRB hyper-phosphorylation and poor survival in HG-SOC

We previously used mESCs to show that OCT4 drives the expression of NIPP1 and CCNF that inhibit the activity of protein phosphatase 1 (PP1) resulting in pRB hyper-phosphorylation and

Figure 1. OCT4 axis promotes poor prognosis in HG-SOC. (**a**) Left panel. Quantitative real-time PCR (qRT–PCR) for *OCT4* (variant A) in human cancer cell lines, normalized to WI38. Right panel, *OCT4* mRNA expression in cancer cell lines (public gene expression database, EGAS00001000610).[48] (**b**) qRT–PCR for *CCNF* and *NIPP1* after transient knockdown of *OCT4* or *NIPP1/CCNF*, normalized to *ACTIN*. Control siRNA value was set '100'. (**c**) Western blotting for phospho-pRB-T356, OCT4, NIPP1 and PP1 after transfection with indicated siRNAs oligos. Numbers represent pRB-T356/ACTIN and NIPP1/ACTIN ratios. (**d**) Western blotting for pRB-T356, OCT4, NIPP1 using OVCAR-3 subclones 11, 4 and 9. Numbers represent pRB-T356/ACTIN and NIPP1/ACTIN ratios. (**e**) Western blotting for pRB-T356, OCT4, NIPP1 in OVCAR-3 subclones 11, 4 and 9 after 3 days of transfection with the indicated siRNAs. Numbers represent pRB-T356/ACTIN and NIPP1/ACTIN ratios. (**f**) Correlating axis gene expression with phosphorylation levels at PP1 target sites pRB-S807 and T356 using the TGCA ovarian cancer data set ($n = 261$). Phosphorylation levels were normalized against overall amount of pRB protein levels. (**g**) Kaplan-Meier survival curve of overall survival (OS) of ovarian cancer patients, classified according to the expression of *CCNF* and *NIPP1* genes (left panel) or *CCNF*, *NIPP1* and *RB1* genes (right panel). Due to the lack of probe-specificity, OCT4 mRNA expression levels were not included in Kaplan–Meier curves. *n*, number of independent experiments; error bars indicate s.d. Linear model regression (**f**); log-rank test (**g**) and one-tail Student's *t*-test were used to calculate significance values: $^{*}P < 0.05$; $^{**}P < 0.01$; $^{***}P < 0.001$. Scale bars correspond to 10 μm.

accelerated cell proliferation[21] (Supplementary Figure 1A). Studying *OCT4* mRNA expression levels in a panel of human cancer cell lines and gene expression data sets, we found that OCT4 reaches highest expression levels in ovarian cancer cell lines and embryonic carcinoma cells (Figure 1a). We therefore studied the role of the OCT4-NIPP1/CCNF-PP1 axis in ovarian cancer. Transient knockdown of *OCT4* using two different types of small intefereing RNAs (siRNAs) in OVCAR-3 cells, a widely used model system for HG-SOC,[27] resulted in reduced expression of OCT4 target genes *NIPP1* and *CCNF,* as detected by quantitative real-time PCT (qRT–PCR) or western blotting using whole cell extracts. Importantly, this effect was paralleled by a reduction of phosphorylation levels at pRB-T356, a reported PP1 target site (Figures 1b and c; Supplementary Figure 1B). Importantly, reduced pRB-T356 phosphorylation was recapitulated by combined knockdown of *NIPP1* and *CCNF* and rescued by depleting *PP1β* in *OCT4* knockdown cells (Figure 1c). Of notice, western blotting using nuclear extracts or immunofluorescence after OCT4 knockdown in OVCAR-3 cells resulted a more pronounced NIPP1 downregulation, indicating that western blotting using whole cell extracts underestimate NIPP1 downregulation in OCT4 depleted OVCAR-3 cells (Supplementary Figure 1C). Results were reproduced in SKOV-3 ovarian cancer cells, underlining the relevance of the OCT4-NIPP1/CCNF-PP1 axis in driving the enzymatic inactivation of pRB in ovarian cancer (Supplementary Figure 1D). The heterogeneity of OCT4 expression in OVCAR-3 cells enabled us to establish single-cell derived subclones that vary in OCT4 expression levels (clone 11 < clone 4 < clone 9) (Figure 1d; Supplementary Figures 1E and F). Of notice, OCT4 expression levels of OVCAR-3 subclones 11, 4 and 9 are considerable lower than expression levels in embryonic stem cells (Supplementary Figure 1G). Using these cell lines, we found that OCT4 expression positively correlates with NIPP1 expression and pRB-T356 phosphorylation (Figures 1d and e). In all subclones, depletion of OCT4 or NIPP1/CCNF reduced pRB-T356 phosphorylation (Figure 1e). The link between *NIPP1/CCNF* or *NIPP1/CCNF/OCT4* levels and pRB phosphorylation at the PP1 target sites pRB-S807 and pRB-T356 was confirmed in large ovarian cancer specimen data sets (Figure 1f). The statistically significant correlation ($P = 0.03$) of RB1 mRNA levels and pRB-S807 and T356 phosphorylation levels in HG-SOC cancer specimen (Supplementary Figure 1H) enabled us to generate Kaplan-Meier survival curves. Importantly, HG-SOC patients with increased *NIPP1/CCNF* expression display a significantly reduced overall survival (OS; $P = 0.008$) that is aggravated when high *RB1* mRNA expression was included into the analysis (OS; $P = 1.39e^{-05}$) (Figure 1g). Altogether, this indicates that the OCT4-NIPP1/CCNF-PP1 axis has clinical relevance for HG-SOC.

The OCT4-NIPP1/CCNF-PP1 axis promotes cell proliferation and tumorigenic potential

We next evaluated the impact of the OCT4-NIPP1/CCNF-PP1 axis on cancer cell proliferation and tumorigenic potential *in vitro*. Transient knockdown of *OCT4* or *NIPP1/CCNF* resulted in significantly decreased BrdU incorporation rates, increased cell doubling time and reduced expression of proliferation markers in OVCAR-3 (Figure 2a; Supplementary Figure 2A). The impact of OCT4, NIPP1 and CCNF on ovarian cancer cell proliferation and BrdU incorporation was confirmed in SKOV-3 cells (Supplementary Figure 2B). Impaired proliferation was recapitulated by treating OVCAR-3 cells with PD 0332991 (Palbociclib), an inhibitor of the Cyclin D-CDK4/CDK6 complex,[28] that controls pRB-T356 phosphorylation (Figure 2a; Supplementary Figure 2C). Of notice, this treatment did not impact on OCT4 or NIPP1 protein levels, thus supporting that PD 0332991 impairs cell proliferation by direct inhibition of CDK4/6 dependent pRB phosphorylation (Supplementary Figure 2C). In line with this, increased OCT4 protein levels in OVCAR-3 subclones 11, 4 and 9 accelerate cell proliferation (Figure 2b). Altogether, this indicates that OCT4 and NIPP1/CCNF promote OVCAR-3 cell proliferation by driving the enzymatic inactivation of pRB. In line with a reported role for OCT4 in enhancing chemoresistance[14,15] we show that progressively increased OCT4 expression enhances the expression of the members of the superfamily of ATP-binding cassette (ABC) transporters, ABCB1 and ABCB10 on the RNA level and mediates enhanced chemoresistance to Cisplatin/Taxol, Doxorubicin, Nocodazole and Actinomycin D (Supplementary Figure 2D). We next investigated *in vitro* tumorigenic potential of OVCAR-3 cells using soft agar colony forming assays. We found that siRNA mediated knockdown of *OCT4* or *NIPP1/CCNF* in OVCAR-3 cells or OVCAR-3 subclones 11, 4, 9 but also PD 0332991 treatment of OVCAR-3 cells resulted in strongly reduced colony number and size (Figure 2c; Supplementary Figure 2E and F). In contrast, transient overexpression of HA-tagged OCT4 or HA-CCNF/NIPP1 significantly increased the tumorigenic potential (Figure 2d; Supplementary Figure 2G). We next tested whether the OCT4-NIPP1/CCNF axis impacts on OVCAR-3 cancer cell spheroid formation, an *in vitro* cell model that resembles ovarian cancer ascites. Remarkably, we found that diameters of control OVCAR-3, stable HA-OCT4 expressing OVCAR-3 cells and OVCAR-3 subclones 11, 4 and 9 correlate with OCT4 proteins expression (Figures 2e and f; Supplementary Figure 2H). Accordingly, loss of OCT4 or NIPP1/CCNF impaired cancer cell sphere formation (Figure 2g; Supplementary Figure 2I; Material and methods section). Altogether, this indicates a critical role for the OCT4-NIPP1/CCNF axis in promoting cell proliferation and tumorigenic potential of HG-SOC cells *in vitro*.

The OCT4-NIPP1/CCNF-PP1 axis promotes mitotic progression

Depletion of *OCT4* or *NIPP1/CCNF* resulted OVCAR-3 cells with flattened morphology and increased β-galactosidase activity (Figures 3a and b; Supplementary Figure 3A). In addition, OCT4 knockdown OVCAR-3 cells showed increased expression of the senescence marker $p16^{INK4A}$ as shown by western blotting experiments but also by immunofluorescence staining that allows

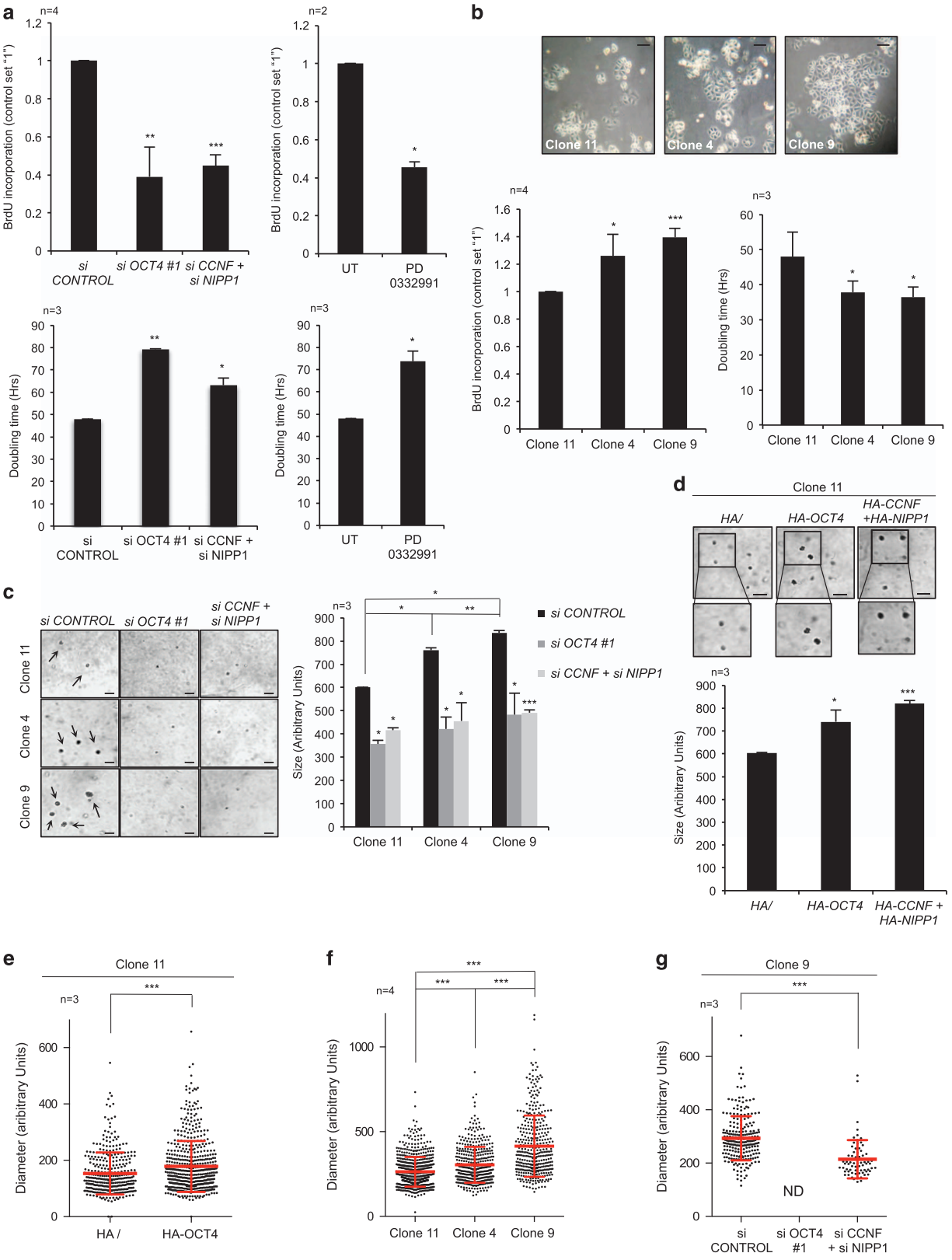

to confront OCT4 and p16^{INK4A} on the single-cell level (Figure 3c, Supplementary Figure 3B and D). In line with this, axis disruption in OVCAR-3 cells, treatment of OVCAR-3 cells with PD 0332991 or low expression OCT4 expression levels in OVCAR-3 subclone 11 was linked with decreased CDK1, cyclin B1 (CCNB1) expression and reduced pRB-T356 phosphorylation levels, further supporting the induction of senescence (Figure 3c; Supplementary Figure 3C). Of notice, PD 0332991 treatment was previously shown to induce

Figure 2. OCT4 axis disruption impairs cell proliferation and tumorigenic potential of OVCAR-3. (**a**) Proliferation was measured by BrdU assay (top) or by calculating doubling time (bottom) after transfection with the indicated siRNAs or treatment with PD 0332991. For BrdU assay, control siRNA value was set '1'. (**b**) Proliferation of OVCAR-3 subclones 11, 4 and 9 was measured by BrdU assay (left) or by calculating doubling time (right). For BrdU assay, clone 11 value was set '1'. Top panel, representative images. (**c**) Colonies size of OVCAR-3 subclones 11, 4 and 9 transiently transfected with the indicated siRNAs oligos and plated in soft agar. Left panel, representative images. Black arrows indicate colonies. (**d**) Soft agar assay of subclones 11 transiently overexpressing *HA-OCT4* or both *HA-CCNF* and *HA-NIPP1* (bottom panel). Top panel, representative images of colonies, including images with higher magnification. (**e**) Diameter of spheroids derived from OVCAR-3 subclone 11 stably overexpressing HA-OCT4. (**f**) Diameter of spheroids derived from OVCAR-3 subclones 11, 4 and 9. (**g**) Diameter of spheroids derived from OVCAR-3 subclone 9 cells transiently transfected with the indicated siRNAs. *n*, number of independent experiments; error bars indicate s.d.; ND, not detected; UT, Untreated; a one-tail Student's *t*-test was used to calculate significance values: $*P < 0.05$; $**P < 0.01$; $***P < 0.001$. Scale bars, 100 μm.

senescence.[29–31] Importantly, increased $p16^{INK4A}$, β-galactosidase activity and pRB-T356 phosphorylation levels as well as reduced cell proliferation of *OCT4* depleted OVCAR-3 cells were partially rescued by ectopic co-expression of HA-tagged NIPP1 and CCNF (Figure 3d; Supplementary Figure 3E). In line with the induction of senescence, we found that acute, siRNA mediated depletion of *OCT4* or *NIPP1/CCNF* for a prolonged period (6 days) caused reduced cell numbers in S, G2/M phases and significantly increased number of cells in G0/G1 phases. This effect is accompanied by increased subG1 numbers and augmented percentage of TUNEL positive cells in OVCAR-3 (Figures 3e and f). SKOV-3 cells recapitulate increased senescence and apoptosis markers upon acute depletion of *OCT4* or NIPP1/CCNF (Supplementary Figure 3F). In order to test whether induction of senescence and apoptosis are regulated in a sequential manner we investigated the expression of marker genes of senescence and apoptosis after 3 and 6 days of RNA interference (RNAi)-mediated depletion of OCT4 or NIPP1/CCNF from OVCAR-3 cells. Western blotting revealed that depletion of OCT4 or NIPP1/CCNF for 6 days results in cleavage of the apoptosis markers Caspase 3 and PARP (Supplementary Figure 3G). Remarkably, $p16^{INK4A}$ is already upregulated after 3 days of OCT4 knockdown (Supplementary Figure 3G). This suggests that in OCT4 knockdown OVCAR-3 cells activation of senescence programs precedes the activation of apoptosis programs. To understand the relative contribution of senescence and apoptosis to the observed cell cycle defects we took advantage of our OVCAR-3 subclones, that show subtle differences in OCT4 and NIPP1/CCNF protein levels. We found that reduced OCT4/NIPP1 expression in OVCAR-3 subclones 11 and 4 significantly reduced S-phase numbers and increased G2/M phase cells indicating defects in mitotic progression (Figure 3g). We conclude that this mitotic phenotype is masked by the induction of apoptosis upon acute depletion of *OCT4* or *NIPP1/CCNF* in transient RNAi experiments (Figures 3e and f; Supplementary Figure 3G). This suggests a new role for OCT4 in stabilizing mitotic progression.

The OCT4-NIPP1/CCNF axis ensures mitotic fidelity by driving the expression of CPC complex

RNAi-mediated depletion of *OCT4* or *NIPP1/CCNF* in OVCAR-3 and SKOV-3 cells caused a significant increased number of micronuclei, indicating genomic instability (Figure 4a; Supplementary Figure 4A). In accordance with this, we found that improved genomic stability in OVCAR-3 subclones 4 and 9 correlates with increased OCT4 expression (Figure 4b). Next, we interrupted the OCT4-NIPP1/CCNF-PP1 axis and studied type and frequency of mitotic spindle defects.[32] RNAi-mediated depletion of *OCT4* or *NIPP1/CCNF* resulted in a 10-fold or 5-fold increase in multipolar spindles, respectively (Figure 4c). OVCAR-3 subclones with low OCT4 expression recapitulated the multipolar spindle phenotype (Figure 4d; Supplementary Figure 4B). Finally, low endogenous OCT4 protein levels or depletion of *OCT4* or *NIPP1/CCNF* significantly increased the frequency of polynucleated OVCAR-3 and SKOV-3 cells, a typical consequence of multipolar spindle formation (Figure 4e; Supplementary Figures 4C and D). Altogether, with previous cell cycle analyses, these data demonstrate that OCT4 and its transcriptional targets NIPP1/CCNF have an unprecedented role in promoting mitotic spindle function. We next knocked-down *OCT4* or *NIPP1/CCNF* in OVCAR-3 cells and performed gene expression profiling experiments to define biological pathway related to mitotic defects. A group of 1153 genes showed common regulation in both *OCT4* and *CCNF/NIPP1* depleted cells (1.4-fold up- or downregulated, $P < 0.05$) (Figure 4f). This indicates that NIPP1 and CCNF have a central role in executing gene expression programs triggered by OCT4. Ingenuity Pathway Analysis (IPA) and GSEA gene ontology on genes that are downregulated upon *OCT4* or *NIPP1/CCNF* depletion identified defects in pathways linked to mitotic progression (Figure 4g). Deeper analysis using the Ingenuity Path Explorer tool highlighted the central components of the Chromosomal Passenger Complex (CPC) Aurora B (AURKB), Survivin (BIRC5), Borealin (CDCA8) and INCENP as downstream targets of the OCT4-NIPP1/CCNF axis (Figure 4h). OCT4 and NIPP1/CCNF dependence of CPC component expression was validated by quantitative RT–PCR (Supplementary Figure 4E). These data suggest that OCT4 and NIPP1/CCNF enhance mitotic stability by driving the expression of CPC complex components.

OCT4 and CCNF/NIPP1 are essential to ensure chromosomal passenger complex function

The chromosomal passenger complex (CPC) is a central regulator of mitosis.[33] During mitosis, the CPC shows specific spatio-temporal localization at different regions along chromosomes, regulating central steps in mitotic progression such as the rescue of errors of chromosome-microtubule attachments, the spindle assembly checkpoint and cytokinesis. Upon entry into mitosis, Aurora B phosphorylates histone H3 at serine 10 (H3-Ser10) and serine 28 (H3-Ser28). This causes the dissociation of Aurora B from HP1 along chromosomal arms and finally allows the concentration of the CPC at inner centromeres to ensure the maintenance of the spindle assembly checkpoint.[33,34] Impairment of CPC function results in abnormal mitotic spindles and defects in mitotic checkpoint control.[35] RNAi-mediated depletion of *OCT4* or *NIPP1/CCNF* in OVCAR-3 and SKOV-3 cells resulted in a drastic reduction of Aurora B protein levels and a concomitant decrease of phosphorylation at Ser10 and Ser28 of histone H3 (Figure 5a; Supplementary Figures 5A and B). RNAi-mediated depletion of *OCT4* or *NIPP1/CCNF* also caused a reduction of Aurora B and H3-Ser10 phosphorylation signal-intensity on metaphase chromosomes as well as defective centromeric concentration of Aurora B and H3-Ser10 phosphorylation, indicative for impaired CPC regulation (Figure 5b). Western blotting data from OVCAR-3 subclones demonstrate that OCT4 protein levels positively correlate with Aurora B expression and H3-Ser10 and H3-Ser28 phosphorylation levels (Figure 5c). In line with this, we observed reduced phosphorylation of

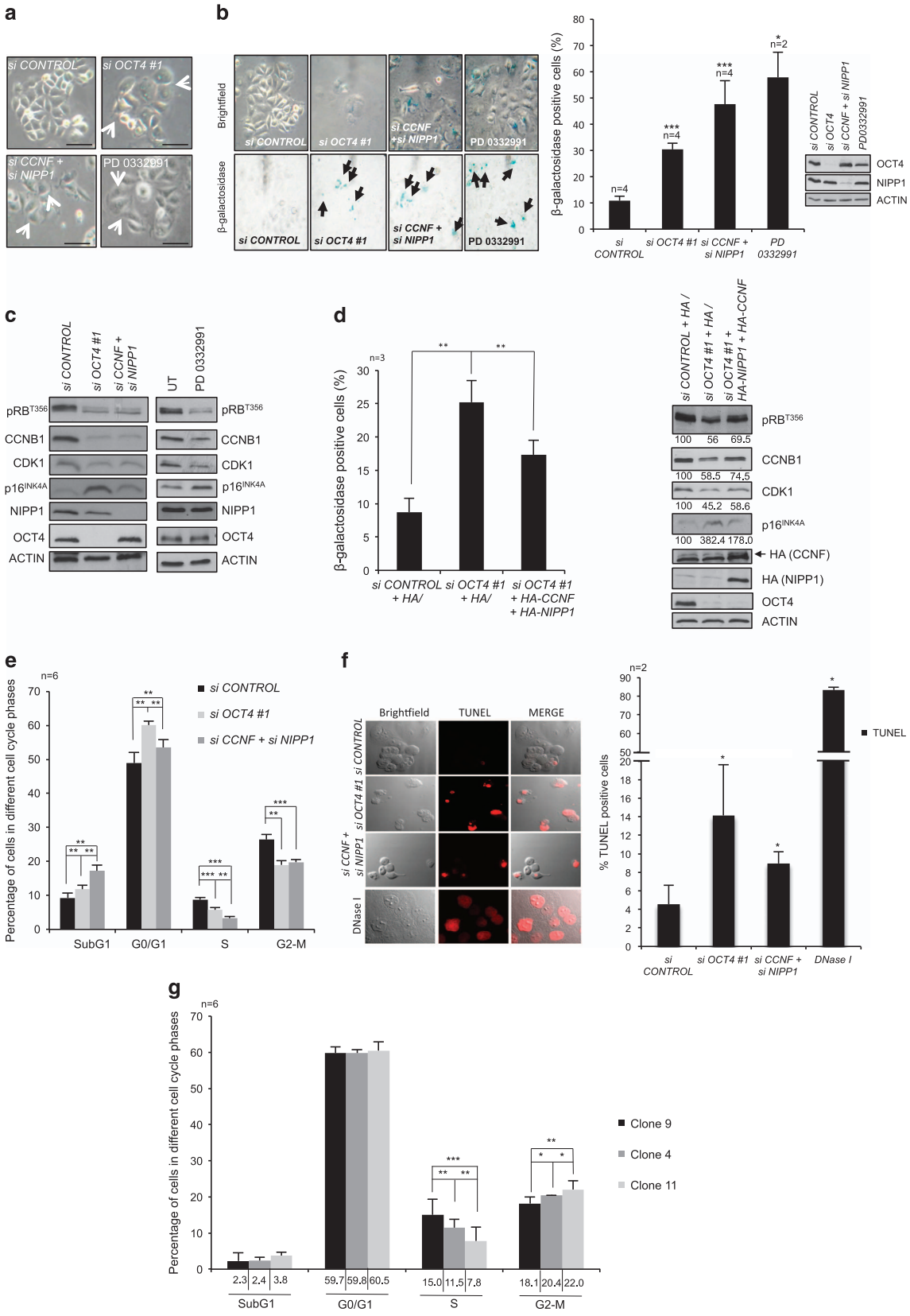

recombinant GST-tagged histone H3 in *in vitro* kinase assays using anti-Aurora B immunoprecipitates obtained from control and OCT4 knockdown OVCAR-3 cells (Figure 5d). Altogether, this indicates that OCT4 has an important role in controlling Aurora B and CPC function. Importantly, reduced global levels of Aurora B and phosphorylated H3-Ser10/Ser28 in *OCT4* depleted cells was rescued by ectopic expression of NIPP1/CCNF (Figure 5e).

Figure 3. OCT4 axis protects from senescence and apoptosis by ensuring mitotic progression. (**a**) Morphology of OVCAR-3 cells transfected with the indicated siRNAs oligonucleotides or treated with PD 0332991. White arrows indicate cells with altered morphology. (**b**) Representative images (left) and quantification of senescence-associated β-galactosidase (SA β-gal) positive cells (middle) as described in **a**. Western blotting of OCT4 and NIPP1 protein levels in experimental cells (right panel). (**c**) Senescence markers in OVCAR-3 cells transiently transfected with the indicated siRNAs oligos or treated with PD 0332991, as detected by western blotting using the indicated antibodies (**d**) Rescuing of senescence phenotype in OCT4 knockdown cells transfected with *HA-CCNF* and *HA-NIPP1* as determined by SA β-gal positive cells (left) or western blotting (right). (**e**) Cell cycle profile of experimental cells, transfected with siRNAs for 6 days. (**f**) TUNEL assay in cells transfected with siRNAs targeting *OCT4* or *NIPP1/CCNF* for longer time (6 days). Left panel, representative images. DNase I treated cells were used as a positive control. (**g**) Cell cycle profile of OVCAR-3 subclones, as determined by FACS analysis. Numbers represent the percentage of cells in different cell cycle phases. n, number of independent experiments; error bars indicate s.d.; UT, Untreated; a one-tail Student's *t*-test was used to calculate significance values: $*P < 0.05$; $**P < 0.01$; $***P < 0.001$. Scale bars, 100 μm.

The NIPP1/CCNF target, Protein Phosphatase 1 (PP1) is reported to de-phosphorylate and inactivate Aurora B and also competes with Aurora B to control phosphorylation levels of histone H3-Ser10 and H3-Ser28.[36] Importantly, we were able to rescue H3-Ser10 and Ser28 phosphorylation in *OCT4* depleted OVCAR-3 cells by treating experimental cells with the PP1 inhibitor Okadaic acid (Supplementary Figure 5C). In line with the role of PP1 in controlling pRB phosphorylation levels we found that Okadaic acid treatment was also able to partially rescue pRB phosphorylation levels in OCT4 depleted OVCAR-3 cells (Supplementary Figure 5C). This provides evidence that OCT4 and its target genes NIPP1/CCNF enhance the expression of CPC components but also enhance pRB phosphorylation and Aurora B activity by suppressing PP1 function. The CPC controls spindle tension at kinetochores and prevents the formation of multipolar spindles and enlarged polyploid cells by promoting the clustering of supernumerary centrosomes.[37] In line with this, we found that reduction of *OCT4* and *NIPP1/CCNF* expression levels causes a prominent increase in the frequency of cells with supernumerary centrosomes and the increased numbers of polynucleated cells (Figures 4e and 5f Supplementary Figure 5D).

Ectopic expression of HA-tagged OCT4 in MDA-MB-231 basal type breast cancer cells that show very low endogenous OCT4 expression, resulted in increased NIPP1, CCNF, Aurora B expression and H3-Ser10 phosphorylation levels (Supplementary Figures 5E and F). Accordingly, loss of OCT4 or NIPP1/CCNF results in a significant reduction of pRB phosphorylation, reduced Aurora B expression and reduced phosphorylation of histone H3-Ser10 and pRB-T356 (Supplementary Figure 5G). FACS analysis of *OCT4* or *NIPP1/CCNF* knockdown MDA-MB-231 reproduced cell cycle alterations observed under the same conditions in OVCAR-3 cells (Supplementary Figure 5H). In line with data from OVCAR-3 cells, overexpression of YFP-tagged OCT4 in MDA-MB-231 is linked with a reduced frequency of micronuclei, polynucleated cells and supernumerary centrosomes (Figures 5g–i; Supplementary Figure 5I). Finally, OCT4 overexpression increases the size of MDA-MB-231 cancer cell spheroids (Figure 5j; Supplementary Figure 5J). This demonstrates that the self-renewal transcription factor OCT4 and its downstream targets NIPP1/CCNF have a general relevance for human cancer genome stability by enhancing CPC function during mitosis.

OCT4-CCNF/NIPP1 axis correlates with CPC activation and poor prognosis in HG-SOC

We next investigated whether the OCT4-CCNF/NIPP1-PP1 axis impinges on pRB phosphorylation and CPC component expression in HG-SOC cancer specimen. The majority of ovarian cancer gene expression data sets do not provide reliable information on *OCT4* mRNA expression.[38] We consequently established a collection of 23 cancer specimens obtained from HG-SOC patients and examined the expression of *OCT4*, *NIPP1*, *CCNF*, *AURKB*, *BIRC5* and *CDCA8 (Borealin)* mRNA by quantitative RT–PCR and immunohistochemistry (IHC) (Supplementary Figure 6A). We used the z-score allocation of *OCT4* mRNA expression levels to subdivide patients in 'OCT4 high' and 'OCT4 low' subgroups (Figures 6a and b; Supplementary Figure 6A). Immunohistochemistry showed that 4 out of 6 cancer samples classified as '*OCT4* mRNA high' contain OCT4 positive cells (ranging from 5 to 50%) with high staining intensity (Figure 6b; Supplementary Figure 6A). In two cancer specimens, high OCT4 mRNA levels do not correlate with data from OCT4 immunohistochemistry, although AURKB, NIPP1 and pRB-T56 phosphorylation was robustly detected by immunohistochemistry. Thus, we suggest that in these samples OCT4 protein is presumably present, but below the detection limit of OCT4 immunohistochemistry (Supplementary Figure 6A). 10 out of 11 specimen classified as '*OCT4* mRNA low' are devoid of OCT4 protein expressing cells (Figure 6b; Supplementary Figure 6A). Western blotting confirmed increased OCT4 protein levels in specimen previously categorized as '*OCT4* mRNA high' by RT–PCR (Supplementary Figure 6B). In line with data from cell line experiments, we found that high *OCT4* mRNA expression is associated with significantly increased *AURKB*, *BIRC5* and *CDCA8 (Borealin)* mRNA levels (Figure 6c). Immunohistochemistry (IHC) revealed that '*OCT4* high' specimen displayed a strongly increased number of NIPP1, phospho-pRB-T356 and AURKB positive cells as well as increased staining intensity (Figures 6d–f; Supplementary Figures 6A and B). We conclude that immunohistochemistry appears as a more stable method to evaluate activity of the OCT4-NIPP1/CCNF axis, as demonstrated by a robust increase of NIPP1 in IHC, compared to quantitative RT–PCR (Figure 6c and e). Importantly, we found that transient knockdown of OCT4 in short term *in vitro* culture of cancer cells obtained from two different HG-SOC tumors caused a reduction of NIPP1, AURKB expression that is paralleled by reduced pRB-T356 and H3-Ser10 phosphorylation levels (Figure 6g). NIPP1/CCNF knockdown cultures reproduced the reduced pRB and H3-Ser10 phosphorylation (Figure 6g). We conclude that the OCT4-NIPP1/CCNF axis is also active in primary human HG-SOC tumor cells. Using mRNA expression data to build Kaplan-Meier survival curves we found that the '*OCT4* high' group of our cohort displays a dramatically reduced overall survival compared to '*OCT4* low' HG-SOC patients (Figure 6h; Supplementary Figure 6A). Importantly, poor overall survival is aggravated when high *OCT4* expression was combined with increased mRNA expression of *AURKB* or *CDCA8* (Figure 6i). This indicates that increased expression of CPC components, activated by OCT4 and NIPP1/CCNF, results an aggressive subtype of HG-SOC. Finally, Kaplan-Meier survival analysis performed on a large HG-SOC ovarian cancer data set confirmed poor overall survival of patients with high expression of all axis and CPC components but also when only considering core genes *NIPP1*, *RB1* and *AURKB* (Figures 6j and k).

Altogether our data indicate that expression of OCT4 and NIPP1/CCNF enzymatically inactivate pRB and enhance CPC

component expression in HG-SOC. This new mechanism enhances mitotic stability and protects cancer cells from increased risk of chromosome instability (CIN) associated with the inactivation of RB tumor suppressor pathway (Figure 7). The poor survival of HG-SOC patients with elevated expression of OCT4, NIPP1/CCNF and downstream CPC targets suggest that

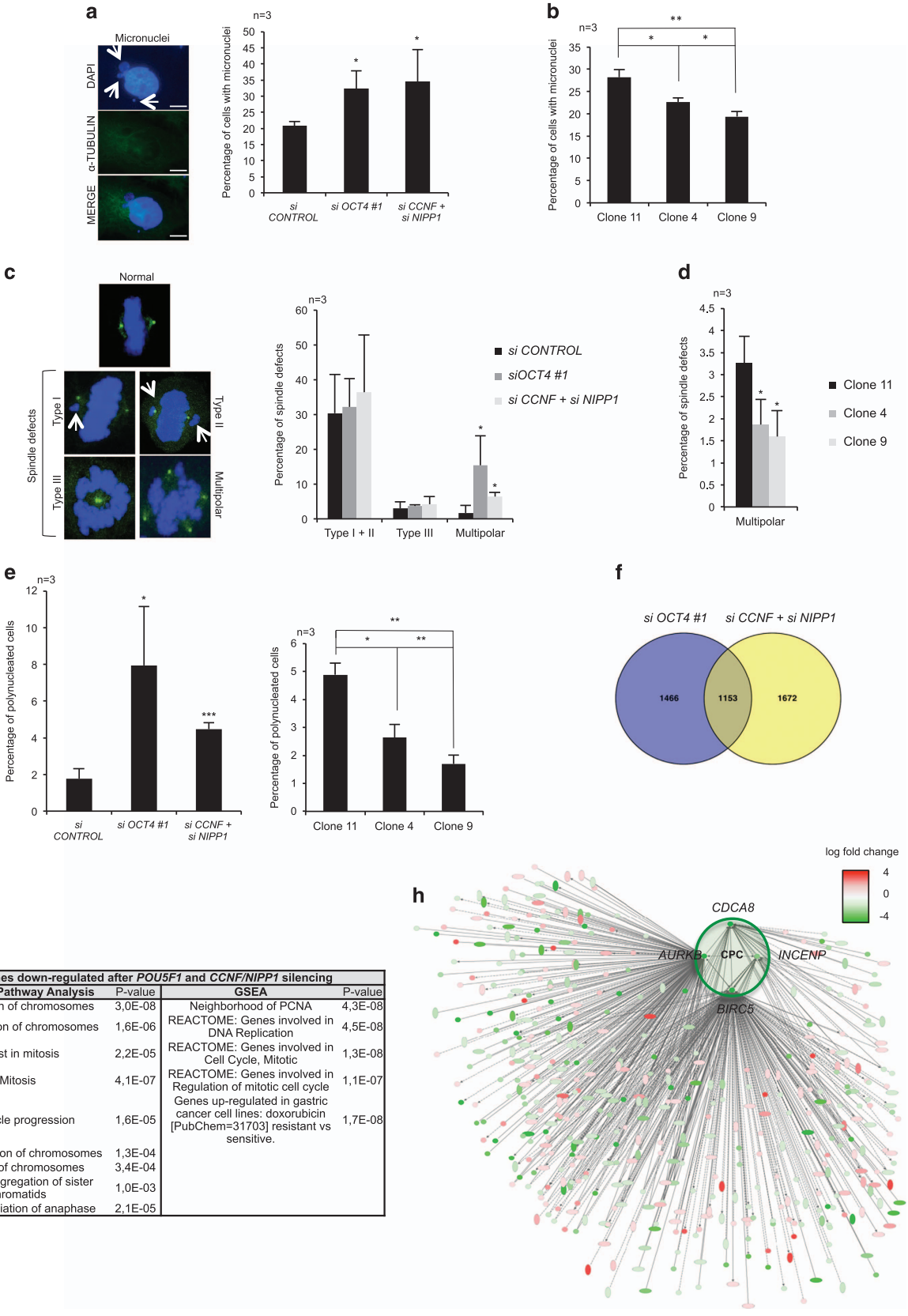

Genes down-regulated after *POU5F1* and *CCNF/NIPP1* silencing			
Ingenuity Pathway Analysis	P-value	**GSEA**	P-value
Segregation of chromosomes	3,0E-08	Neighborhood of PCNA	4,3E-08
Condensation of chromosomes	1,6E-06	REACTOME: Genes involved in DNA Replication	4,5E-08
Arrest in mitosis	2,2E-05	REACTOME: Genes involved in Cell Cycle, Mitotic	1,3E-08
Mitosis	4,1E-07	REACTOME: Genes involved in Regulation of mitotic cell cycle	1,1E-07
Cell cycle progression	1,6E-05	Genes up-regulated in gastric cancer cell lines: doxorubicin [PubChem=31703] resistant vs sensitive.	1,7E-08
Missegregation of chromosomes	1,3E-04		
Quantity of chromosomes	3,4E-04		
Delay in segregation of sister chromatids	1,0E-03		
Delay in initiation of anaphase	2,1E-05		

disrupting the OCT4-NIPP1/CCNF-PP1/Aurora B axis represents a promising strategy to target an aggressive subpopulation of HG-SOC cells.

DISCUSSION

OCT4 promotes cancer formation and progression and is linked with poor clinical outcome.[5–12,14,15] Using HG-SOC as model system we found that OCT4 drives the expression of NIPP1 and CCNF, both reported enzymatic inhibitor of Protein Phosphatase 1 (PP1) resulting in pRB hyper-phosphorylation and enhanced proliferation. Importantly, this pathway was also found to be active in cancer cells that were directly cultured from HG-SOC tumors. HG-SOC gene expression data sets link this pathway with poor patient overall survival. This suggests that OCT4, NIPP1 and CCNF are relevant factors that contribute to the enzymatic inactivation of the RB tumor suppressor pathway, observed in 70% of HG-SOC tumors.[39] We further report that expression of *OCT4* and its downstream target genes *NIPP1/CCNF* protect ovarian cancer cell from defects in G2/M progression, senescence, apoptosis and promotes chemoresistance and *in vitro* cell invasiveness. The classic role of OCT4 in promoting self-renewal appears suggestive for an eventual function of the OCT4-NIPP1/CCNF axis in cancer stem cell biology. However, additional functional experiments involving advanced preclinical cancer models systems will be necessary to investigate a role of these proteins in defining cancer stem cell potential in HG-SOC. Here we focus our research on a novel role of OCT4 in promoting mitotic stability. Using HG-SOC (OVCAR-3, SKOV-3) and breast cancer cells (MDA-MB-231) as cancer model systems we found that disruption of the OCT4-NIPP1/CCNF axis is paralleled by the appearance of severe mitotic defects, including the formation of micronuclei, multipolar spindles, supernumerary centrosomes and polynucleated cells. This highlights the general relevance of the OCT4-NIPP1/CCNF axis in enhancing mitotic stability of cancer cells.

The classic role of Retinoblastoma family proteins is to control G1/S transition by regulating the activity of the E2F transcription factor.[40] However, loss of Retinoblastoma function also provokes mitotic defects including micronuclei formation, centrosome amplification, multipolar spindles and merotelic spindle attachments.[22,23] These defects are explained by the role of Retinoblastoma family proteins in controlling centromeric chromatin structure, DNA damage checkpoints and the impact of a subset of E2F target genes on mitotic regulation.[24–26] How can we explain that OCT4 and NIPP1/CCNF expression promotes the enzymatic inactivation of pRB, but at the same time efficiently increases mitotic stability? Gene expression analysis show that OCT4 and NIPP1/CCNF promote the expression of Aurora B, Borealin and Survivin, key components of the Chromosomal Passenger Complex (CPC) that ensures kinetochore function and centrosome clustering during mitosis.[33,37] Impaired CPC function is reported to drive mitotic spindle aberrations and polyploidy.[35] In line with this, we show that reduced expression of Borealin, Survivin and Aurora B in *OCT4* or *NIPP1/CCNF* depleted OVCAR-3 and other unrelated cancer cell lines impair CPC function, as demonstrated by the low abundance of Aurora B and phosphorylated H3-Ser10 at centromeres of metaphase chromosomes. This staining pattern is compatible with the appearance of supernumerary centrosomes, multipolar spindles and polyploidy in *OCT4* or *NIPP1/CCNF* depleted OVCAR-3 cells. Importantly, Aurora B immunoprecipitates of OCT4 depleted cells showed a reduced kinase activity towards H3-Ser10 *in vitro*, supporting that OCT4 regulates H3-Ser10 phosphorylation of mitotic chromosomes via Aurora B.

Altogether our functional data demonstrate that the self-renewal transcription factor OCT4 activates two parallel pathways: OCT4-NIPP1/CCNF mediates the inhibition of PP1 leading to pRB hyper-phosphorylation, thus accelerating cell proliferation. At the same time, OCT4-NIPP1/CCNF promotes the expression of the CPC components Aurora B, Borealin and Survivin to enhance mitotic stability in cells with impaired tumorsuppression pathways (Figure 7). Of notice, PP1 was reported to inactivate Aurora B by de-phosphorylation and also to compete with Aurora B in controlling phosphorylation levels at histone H3-Ser10.[36] Consequently, inhibition of PP1 by the OCT4-NIPP1/CCNF axis further enhances the regulatory strength of Aurora B during mitotic progression. In line with this we were able to rescue pRB hyper-phosphorylation and H3-Ser10/Ser28 phosphorylation of OCT4 depleted cells by a treatment with the PP1 inhibitor Okadaic acid. The activation of senescence and apoptosis pathways upon inactivation of pRB or Aurora B by OCT4 depletion is in line with recent reports that link pRB and Aurora B loss of function with the protection from senescence and apoptosis.[41–45] Altogether, our mechanistic data highlight a central role of OCT4 in driving cell proliferation by inactivating the pRB pathway and enhancing mitotic stability by ensuring CPC function (Figure 7).

RNA and protein data from a collection of HG-SOC specimen revealed that increased OCT4 expression was linked with an augmented expression of NIPP1, Aurora B, Borealin, Survivin and increased pRB-T356 phosphorylation levels, demonstrating that the OCT4-NIPP1/CCNF axis is also functional in ovarian cancer patients. Poor survival of HG-SOC patients with high OCT4 expression was exacerbated when high OCT4 expression was paired with high Borealin or Aurora B expression. This highlights the relevance of the OCT4-NIPP1/CCNF-PP1 axis in HG-SOC. Remarkably, poor survival of 2 out of 6 patients in the OCT4 mRNA 'high' group was paralleled with a very low percentage of OCT4 positive cells (5%). This suggests that the presence of a small proportion of OCT4 positive cells might already be sufficient to give rise to a particularly aggressive HG-SOC subtype. We thus

Figure 4. OCT4 axis disruption leads to genome instability by down regulating the expression of CPC components. (**a**) Percentage (right) and representative images (left) of micronuclei in OVCAR-3 subclone 9 transiently transfected with siRNAs targeting *OCT4* or *CCNF/NIPP1* (1000 cells were analyzed; arrows show micronuclei). (**b**) Percentage of micronuclei in OVCAR-3 subclones 11, 4 and 9 cells (1000 cells were analyzed). (**c**) Percentage (right) or representative images (left) of type I, II, III and multipolar spindle errors[32] in OVCAR-3 subclone 9 after knockdown of *OCT4* or *CCNF/NIPP1* (100 mitosis were analyzed). (**d**) Quantification of multipolar spindle defects of subclones 11, 4 and 9 (100 mitosis were analyzed). (**e**) Left panel, percentage of polynucleated OVCAR-3 subclone 9 cells after knockdown of *OCT4* or *CCNF/NIPP1* (500 cells were analyzed). Right panel, percentage of polynucleated OVCAR-3 subclones 11, 4 and 9 cells (500 cells were analyzed). (**f**) Venn Diagram showing overlap between differentially expressed genes of OVCAR-3 cells subjected to RNAi-mediated depletion of *OCT4* or *CCNF/NIPP1*. (**g**) Functional annotation of genes downregulated after *OCT4* and *CCNF/NIPP1* knockdown, using the Ingenuity Pathway Analysis tool (IPA) and Gene Set Enrichment Analysis (GSEA). (**h**) Automated literature research using Ingenuity Path Explorer tool using genes subjected to regulation by OCT4-NIPP1/CCNF-PP1 axis. n, number of independent experiments; error bars indicate s.d.; Right tail Fisher's Exact test (**g**) and one-tail Student's *t*-test (all other panels) were used: $*P < 0.05$; $**P < 0.01$; $***P < 0.001$. Scale bars, 10 μm.

propose that OCT4, NIPP1 and CCNF expression in HG-SOC cells might support the formation of a reservoir of cancer cells with stable genetic identity that drive cancer aggressiveness. In line our study, OCT4 expressing ovarian cancer cells were demonstrated to carry cancer initiating potential, high invasive potential and increased chemoresistance.[9,10,17–20,46] Consequently,

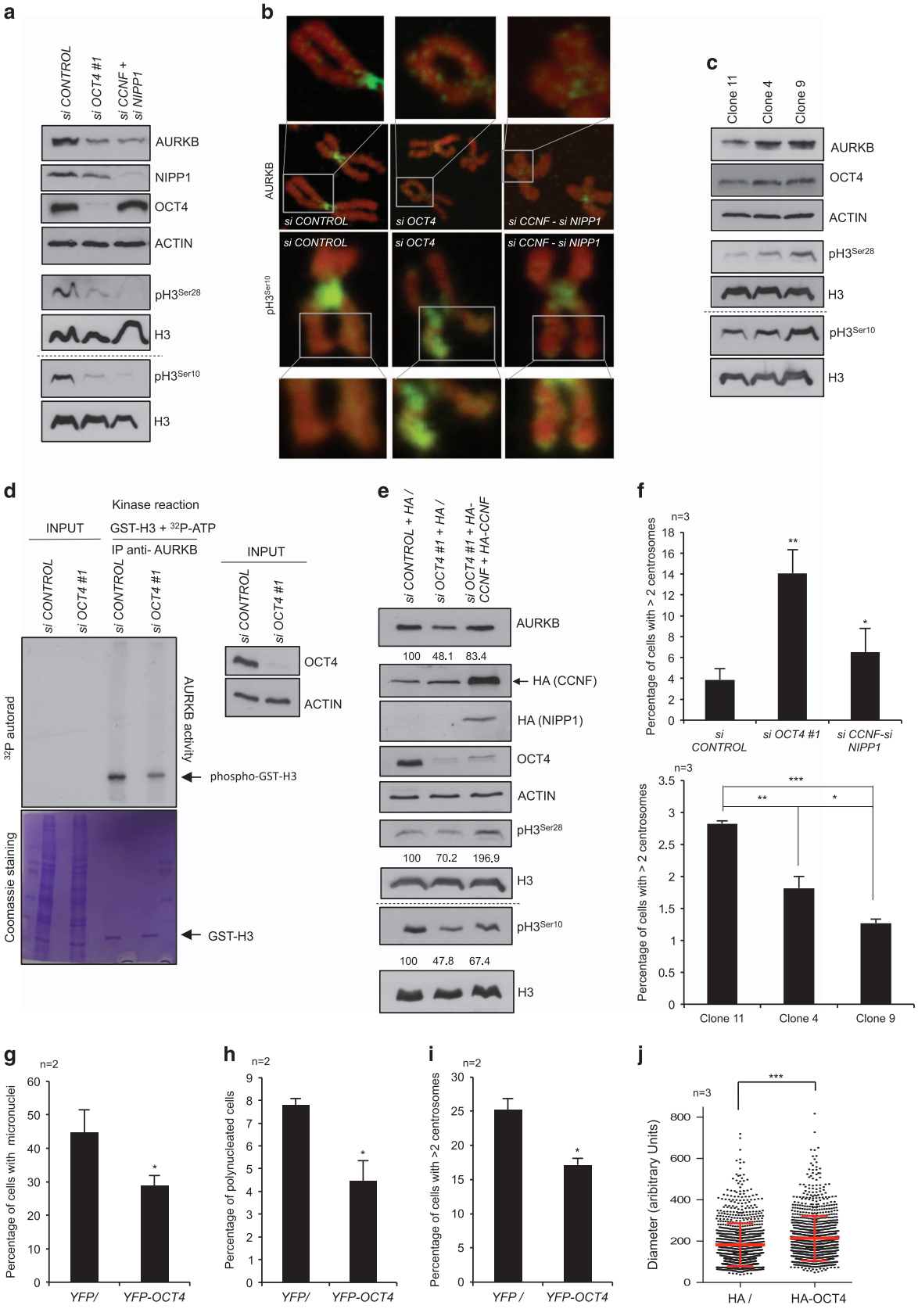

disrupting the OCT4-NIPP1/CCNF-PP1 axis represents an attractive strategy for targeting an aggressive OCT4+ HG-SOC subtype of HG-SOC.

MATERIALS AND METHODS

Cell culture

All cell lines were obtained from ATCC and have not been cultured for longer than 6 months (ATCC characterization by Short Tandem Repeat—STR—analysis) and subjected to mycoplasma test. NIH-OVCAR-3 cells (indicated in the text as OVCAR-3) were cultured in RPMI-1640 medium (Lonza, Basel, Switzerland) supplemented with 20% (v/v) Fetal Bovine Serum (FBS), insulin (10 μg/ml; I9278, Sigma-Aldrich, St Louis, MO, USA) and 1% (v/v) penicillin/streptomycin (Lonza). MDA-MB-231 and SKOV-3 cell lines were maintained in DMEM medium (BioWhittaker, Lonza) supplemented with 10% (v/v) FBS and 1% (v/v) penicillin/streptomycin (Lonza). OVCAR-3 subclones were obtained by plating the cells at a low concentration to pick individual colonies. Stable OVCAR-3 subclone 11 overexpressing HA-OCT4 (Supplementary Methods) were selected using G-418 (100 μg/ml; Sigma-Aldrich). High-Grade Serous Ovarian Cancer (HG-SOC) primary cells were obtained from the Institute of Pathology of the University of Udine after obtaining an informed consent, in accordance with the Declaration of Helsinki, and with approval by the Independent Ethics Committee of the University Hospital of Udine.

Transient transfection of siRNA oligos, plasmids and western blotting

Transient transfections of siRNAs were performed using Lipofectamine RNAiMAX reagent (siRNAs, Invitrogen, Carlsbad, CA, USA) or *Trans*IT-LT1 transfection reagent (plasmids, #MIR-2300, Mirus, Madison, WI, USA). For plasmids, siRNAs targeting sequences and primary antibodies see Supplementary Methods. Whole-cell lysates were prepared 72 h after transfection, unless otherwise specified according to standard procedures.

quantitative real-time PCR

Total RNA was extracted using TRIzol reagent (Invitrogen) and cDNA was generated using QuantiTect Reverse Transcription Kit (Promega, Madison, WI, USA) according to the manufacturer's suggestions. Quantitative RT-PCR (qRT-PCR) was performed using the SYBR Green PCR Master Mix (Applied Biosystem, Foster City, CA, USA) and analyzed with a StepOnePlus real-time PCR machine (Applied Biosystem). For qRT–PCR oligos see Supplementary Methods.

Spheroids formation

Spheroids were generated as previously reported.[47] 50000 OVCAR-3 cells and MDA-MB-231 cells were plated on top of the agarose-coated wells and incubated at 37 °C. After 4 days spheroids were analyzed using ImageJ software (http://imagej.nih.gov/ij/). For RNAi experiments, cells were transfected twice in 6 days period before plating on agar.

Apoptosis and proliferation analysis

Cell cycle analysis was performed by PI staining (Sigma-Aldrich) for DNA content and followed by cytometric analysis (FACSCalibur, Becton Dickinson). FACS data were analyzed using FlowJo software (FlowJo LLC, Ashland, OR, USA). Number of cells plated and detailed procedures for FACS analysis, SA β-gal and BrdU incorporation assays are indicated in Supplementary Methods.

TUNEL assay was performed with *In Situ Cell Death Detection Kit* (TMR red) (Roche, Basel, Switzerland) following manufacturer's instructions. OVCAR-3 cells were plated at a concentration of 6×10^4 cells/ml and transfected with the indicated siRNAs twice in a 6 days period.

Confocal analysis

OVCAR-3 cells were transiently transfected with the indicated siRNA oligonucleotides. Immunofluorescence procedures are described in Supplementary Methods. *Z*-stack sections of each mitosis were acquired using Zeiss LSM 510 Meta confocal microscope and analyzed with ImageJ software (http://imagej.nih.gov/ij/). Nuclei were counterstained with DAPI (4′,6-Diamidino-2-Phenylindole) or propidium iodide (Sigma-Aldrich). For centrosomes, multiple nuclei and micronuclei analysis cells were analyzed on Leica DM 4000B fluorescence microscope. Primary and secondary antibodies used are listed in Supplementary Methods.

In vitro kinase assay

For *in vitro* kinase assays, Aurora Kinase B was immunoprecipitated (rabbit polyclonal anti-Aurora B, ab2254, Abcam, Cambridge, UK) from lysates prepared from siCONTROL and siOCT4 OVCAR-3 subclone 9 cells. 2 μg of purified recombinant GST-histone H3 fusion protein was used as substrate. Kinase reactions were carried out in 30 μl kinase buffer (20 mM HEPES pH 7.0, 10 mM $MgCl_2$, 5 mM β-glycerophosphate, 2 mM DTT, 1 mM sodium orthovanadate, and proteinase inhibitor cocktail) containing 10 μCi of ^{32}P-ATP and 200 μM ATP at 30 °C for 30 min. Products were seperated by SDS-PAGE, stained using Coomassie Brillant Blue (Sigma-Aldrich, B0149) and visualized by autoradiography.

Immunofluorescence of metaphase spreads

Cells arrested in metaphase with 1 μg/ml colcemid (Karyo MAX COLCEMID Solution, Gibco, Thermo Fisher Scientific, Waltham, MA, USA) for 4 h were collected and resuspended in 0.2% (w/v) and 0.2% (w/v) trisodium citrate hypotonic buffer for 15 min. Cells were then spun onto glass slides using a centrifuge (Cytospin, Cytopro, Wescor) at 2000 rpm for 4 min, fixed in 4% paraformaldehyde for 10 min, permeabilized in KCM buffer (120 mM KCl, 20 mM NaCl, 10 mM Tris (pH 7.5) and 0.1% Triton X-100) and processed for indirect immunofluorescence. Primary and secondary antibodies used are listed in Supplementary Methods.

Microarray hybridization and low level analysis

Gene expression profiling was performed using Illumina HumanHT-12-v4-BeadChips according to the manufacturer's suggestions. RNA of OVCAR-3 cells transfected with OCT4 or CCNF/NIPP1 siRNAs was prepared 6 days after transfection. The probe intensities were calculated and normalized using GenomeStudio Data Analysis Software's Gene Expression Module (GSGX) Version 1.9 (Illumina, San Diego, CA, USA). Further data processing was performed in the R computing environment (http://www.r-project.org/) version 3.1, with BioConductor packages (http://www.bioconductor.org/). Statistical analysis for differentially expressed genes

Figure 5. OCT4 axis controls CPC expression and function. (**a**) Western blotting analysis of OVCAR-3 cells after *OCT4* and *CCNF/NIPP1* knockdown using the indicated antibodies. (**b**) Immunofluorescence analysis of metaphase spreads of OVCAR-3 subclone 9 cells transiently transfected with the indicated siRNAs oligos. (**c**) Western blotting analysis of OVCAR-3 subclones 11, 4 and 9 using the indicated antibodies. (**d**) *In vitro* kinase assay using recombinant GST-H3 and Aurora B kinase immunoprecipitated from OVCAR-3 subclone 9 cells after transient knockdown of *OCT4*. Autoradiogram (top panel) and Coomassie-stained gel (bottom panel) are shown. Right panel, western blotting of OCT4 protein expression demonstrating siRNA silencing efficiency. (**e**) Western blotting of subclone 9 OVCAR-3 cells transiently transfected with siRNAs targeting *OCT4* or cotransfected with *OCT4* siRNAs and *HA-CCNF* and *HA-NIPP1* expression vectors. Used antibodies are indicated. Numbers represent pRB-T356/ACTIN and pH3-Ser10/Ser28/ACTIN ratios. (**f**) Top panel, Percentage of cells transfected with indicated siRNAs that show more than 2 centrosomes (200 cells were analyzed). Bottom panel, Percentage of cells showing more than 2 centrosomes in OVCAR-3 subclones 11, 4 and 9 (500 cells were analyzed). (**g**–**i**) MDA-MB-231 cells were transfected as indicated: percentage of cells with micronuclei (**g**), polynucleated (**h**) or with more than 2 centrosomes (**i**) (100 cells were analyzed). A YFP-empty vector was used as control. (**j**) Cell spheroid diameter of MDA-MB-231 cells stably expressing HA-OCT4. n, number of independent experiments; error bars indicate s.d.; a one-tail Student's *t*-test was used to calculate significance values: $^*P < 0.05$; $^{**}P < 0.01$; $^{***}P < 0.001$. PI, propidium iodide. Scale bars, 10 μm.

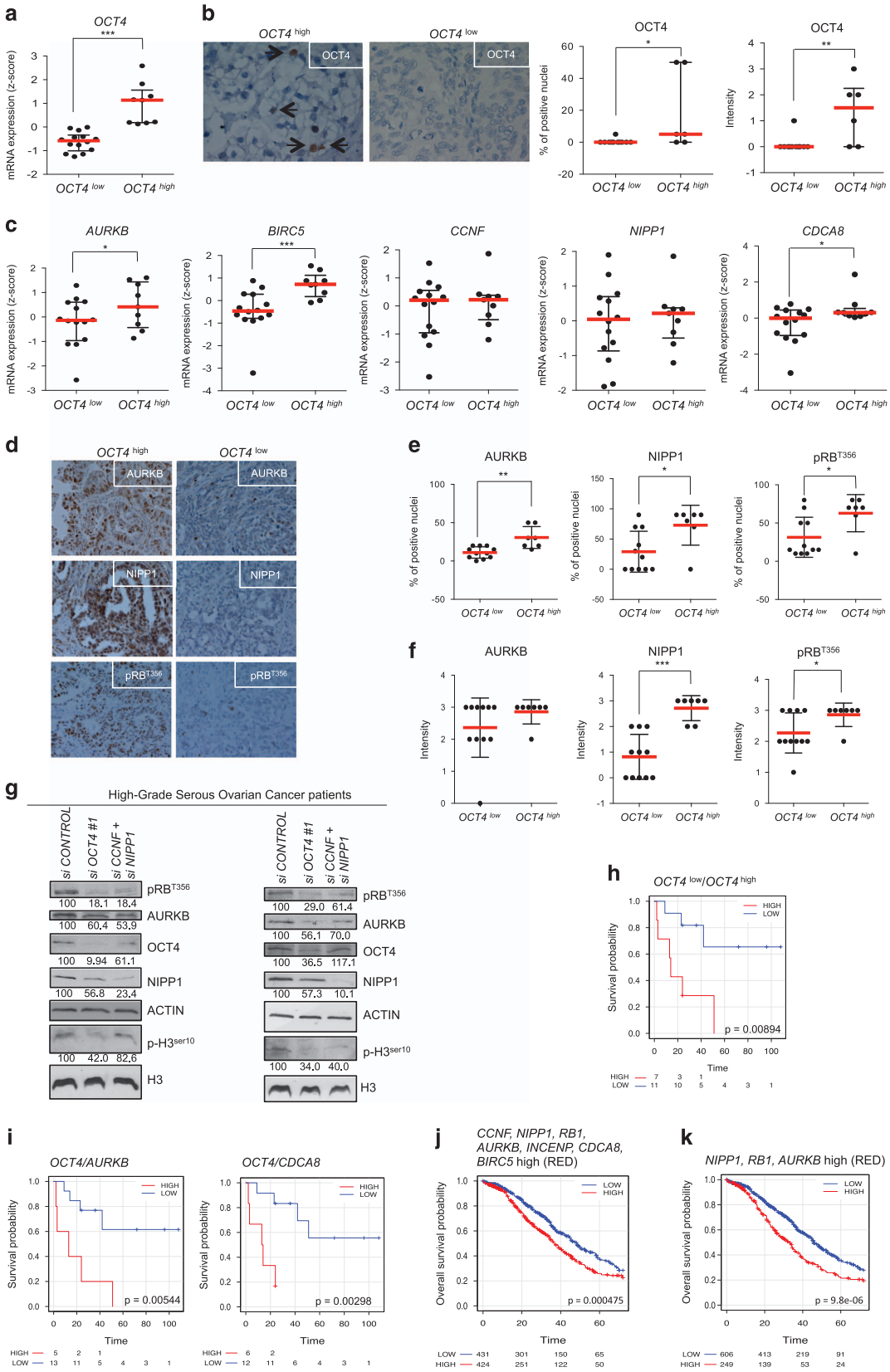

was performed with limma. *P*-values were adjusted for multiple testing using Benjamini and Hochberg's method to control the false discovery rate. Microarray data were submitted to the GEO repository (GEO accession number GSE76689).

Statistical analysis

Statistical analysis and graphical representation have been performed using R statistical environment. Significance of the difference between the means of the experimental conditions and control has been calculated

Figure 6. OCT4 axis activity correlates with increased CPC expression and poor prognosis in HG-SOC patients. (**a**) Allocation of HG-SOC patient specimens into 'high' or 'low' mRNA *OCT4* expression, according to z-score analysis. Red line represents median value. (**b**) Left panel, OCT4 immunohistochemistry analysis of two representative samples (OCT4 high: B2011.16594 and OCT4 low: B2007.13711). Right panel, percentage of OCT4 positive cells in HG-SOC specimens. Red line represents mean value. (**c**) qRT–PCR for *CCNF*, *NIPP1* and CPC components in HG-SOC patients grouped into '*OCT4* mRNA high' and '*OCT4* low mRNA' expression (see (**a**)). Red line represents median value. (**d**) Immunohistochemistry of HG-SOC patient specimen for Aurora B, NIPP1 and pRB-T356. Specimens were classified according to *OCT4* expression levels. (**e** and **f**) IHC on cancer specimens using the indicated antibodies; percentage of IHC-positive cells (**e**) and staining intensity (**f**). Samples were classified according to *OCT4* expression levels. Red line represents mean value. (**g**) Western blotting of two primary HG-SOC cell pools transiently transfected with siRNAs targeting *OCT4* and *CCNF/NIPP1*. Expression of pRB-T356, AURKB, OCT4, NIPP1 and H3-Ser10 was monitored. ACTIN and H3 were used as loading control. Numbers represent pRB-T356/ACTIN, AURKB/ACTIN, OCT4/ACTIN, NIPP1/ACTIN and p-H3-Ser10/H3 ratios. (**h**) Kaplan-Meier overall survival curve of HG-SOC patients grouped into 'OCT4 high' or 'OCT4 low' subgroups according to *OCT4* mRNA levels. Only patients with more than 36 months of follow-up were included in the analysis. (**i**) Kaplan-Meier overall survival curves of HG-SOC patients grouped according to *OCT4* or combined *OCT4*/CPC components expression. (**j**) Kaplan-Meier overall survival curves of 850 high-grade serous ovarian cancer specimens, classified according to their *CCNF*, *NIPP1*, *RB1*, *AURKB* (Aurora B), *INCENP*, *CDCA8* (Borealin) and *BIRC5* (Survivin) expression. (**k**) Kaplan–Meier overall survival curve of 850 high-grade serous ovarian cancer patients according to their *NIPP1*, *RB1*, *AURKB* expression. n, number of independent experiments carried out; error bars indicate s.d.; a one-tail Welch's *T*-test (**a** and **c**), a one-tail Student *t*-test (**b**, **e** and **f**) and Log-Rank test (**h**–**k**) were used to calculate significance values: $*P < 0.05$; $**P < 0.01$; $***P < 0.001$.

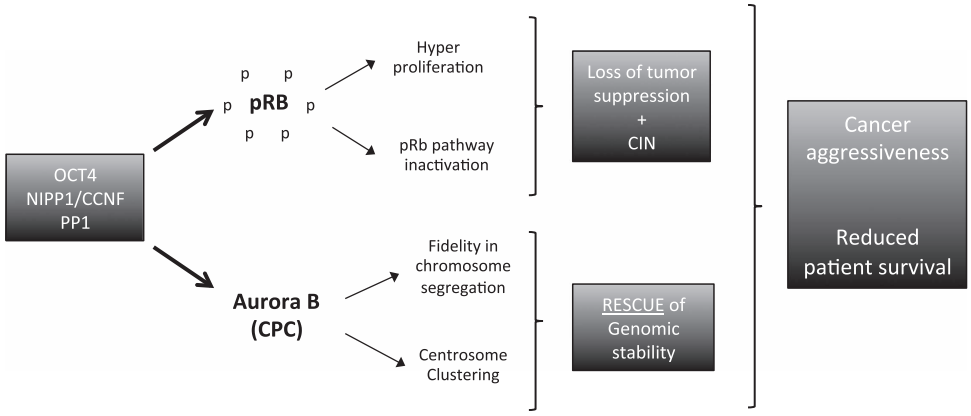

Figure 7. Model describing the impact of the OCT4 axis on the RB pathway and mitotic stability in HG-SOC.

performing a paired Student's *t*-test. *P*-values are shown. In bar plots, error bars represent standard deviation. Each finding was confirmed by at least three independent biological replicates, unless differently specified.

CONFLICT OF INTEREST

The authors declare no conflict of interest.

ACKNOWLEDGEMENTS

We thank Angelica Feresin and Simone Pisano (University of Udine, Italy) for helping with processing of patient samples and with spindle defects experiments. EC and MS are AIRC post-doctoral fellows. MR is enrolled in the PhD program for Molecular Medicine at the University of Trieste. This work was supported by an AIRC grant (Rif 17756 to RB and Rif 10299 to SS), a financial support by the Rotary Club Bari Sud to RB and a grant from the Italian Ministry of Education, Universities and Research (MIUR) CTN01_00177_817708 to CS.

REFERENCES

1 Tantin D. Oct transcription factors in development and stem cells: insights and mechanisms. *Development* 2013; **140**: 2857–2866.
2 Gidekel S, Pizov G, Bergman Y, Pikarsky E. Oct-3/4 is a dose-dependent oncogenic fate determinant. *Cancer Cell* 2003; **4**: 361–370.
3 Hochedlinger K, Yamada Y, Beard C, Jaenisch R. Ectopic expression of Oct-4 blocks progenitor-cell differentiation and causes dysplasia in epithelial tissues. *Cell* 2005; **121**: 465–477.
4 Darini CY, Pisani DF, Hofman P, Pedeutour F, Sudaka I, Chomienne C *et al.* Self-renewal gene tracking to identify tumour-initiating cells associated with metastatic potential. *Oncogene* 2012; **31**: 2438–2449.
5 Zhao P, Liu C, Xu K, Zheng S, Li H, Xu Y *et al.* [Expression of OCT4 protein in bladder cancer and its clinicopathological implications]. *Nan Fang Yi Ke Da Xue Xue Bao* 2012; **32**: 643–646.
6 Huang P, Chen J, Wang L, Na Y, Kaku H, Ueki H *et al.* Implications of transcriptional factor, OCT-4, in human bladder malignancy and tumor recurrence. *Med Oncol* 2012; **29**: 829–834.
7 Chen Z, Wang T, Cai L, Su C, Zhong B, Lei Y *et al.* Clinicopathological significance of non-small cell lung cancer with high prevalence of Oct-4 tumor cells. *J Exp Clin Cancer Res* 2012; **31**: 10.
8 Chen Y-C, Hsu H-S, Chen Y-W, Tsai T-H, How C-K, Wang C-Y *et al.* Oct-4 expression maintained cancer stem-like properties in lung cancer-derived CD133-positive cells. *PLoS ONE* 2008; **3**: e2637.
9 Hu L, McArthur C, Jaffe RB. Ovarian cancer stem-like side-population cells are tumourigenic and chemoresistant. *Br J Cancer* 2010; **102**: 1276–1283.
10 Vathipadiekal V, Saxena D, Mok SC, Hauschka P V, Ozbun L, Birrer MJ. Identification of a potential ovarian cancer stem cell gene expression profile from advanced stage papillary serous ovarian cancer. *PLoS ONE* 2012; **7**: e29079.
11 Levings PP, McGarry S V, Currie TP, Nickerson DM, McClellan S, Ghivizzani SC *et al.* Expression of an exogenous human Oct-4 promoter identifies tumor-initiating cells in osteosarcoma. *Cancer Res* 2009; **69**: 5648–5655.
12 Koo BS, Lee SH, Kim JM, Huang S, Kim SH, Rho YS *et al.* Oct4 is a critical regulator of stemness in head and neck squamous carcinoma cells. *Oncogene* 2015; **34**: 2317–2324.
13 Hu T, Liu S, Breiter DR, Wang F, Tang Y, Sun S. Octamer 4 small interfering RNA results in cancer stem cell-like cell apoptosis. *Cancer Res* 2008; **68**: 6533–6540.
14 Wang XQ, Ongkeko WM, Chen L, Yang ZF, Lu P, Chen KK *et al.* Octamer 4 (Oct4) mediates chemotherapeutic drug resistance in liver cancer cells through a potential Oct4-AKT-ATP-binding cassette G2 pathway. *Hepatology* 2010; **52**: 528–539.
15 Linn DE, Yang X, Sun F, Xie Y, Chen H, Jiang R *et al.* A role for OCT4 in tumor initiation of drug-resistant prostate cancer cells. *Genes Cancer* 2010; **1**: 908–916.

16 Dai X, Ge J, Wang X, Qian X, Zhang C, Li X. OCT4 regulates epithelial-mesenchymal transition and its knockdown inhibits colorectal cancer cell migration and invasion. *Oncol Rep* 2013; **29**: 155–160.
17 Zhang J, Li Y-L, Zhou C-Y, Hu Y-T, Chen H-Z. Expression of octamer-4 in serous and mucinous ovarian carcinoma. *J Clin Pathol* 2010; **63**: 879–883.
18 Bapat SA, Mali AM, Koppikar CB, Kurrey NK. Stem and progenitor-like cells contribute to the aggressive behavior of human epithelial ovarian cancer. *Cancer Res* 2005; **65**: 3025–3029.
19 Gao M-Q, Choi Y-P, Kang S, Youn JH, Cho N-H. CD24+ cells from hierarchically organized ovarian cancer are enriched in cancer stem cells. *Oncogene* 2010; **29**: 2672–2680.
20 Latifi A, Luwor RB, Bilandzic M, Nazaretian S, Stenvers K, Pyman J *et al.* Isolation and characterization of tumor cells from the ascites of ovarian cancer patients: molecular phenotype of chemoresistant ovarian tumors. *PLoS ONE* 2012; **7**: e46858.
21 Schoeftner S, Scarola M, Comisso E, Schneider C, Benetti R. An Oct4-pRb axis, controlled by MiR-335, integrates stem cell self-renewal and cell cycle control. *Stem Cells* 2013; **31**: 717–728.
22 Amato A, Lentini L, Schillaci T, Iovino F, Di Leonardo A. RNAi mediated acute depletion of retinoblastoma protein (pRb) promotes aneuploidy in human primary cells via micronuclei formation. *BMC Cell Biol* 2009; **10**: 79.
23 Iovino F, Lentini L, Amato A, Di Leonardo A. RB acute loss induces centrosome amplification and aneuploidy in murine primary fibroblasts. *Mol Cancer* 2006; **5**: 38.
24 Bester AC, Roniger M, Oren YS, Im MM, Sarni D, Chaoat M *et al.* Nucleotide deficiency promotes genomic instability in early stages of cancer development. *Cell* 2011; **145**: 435–446.
25 Schvartzman J-M, Duijf PHG, Sotillo R, Coker C, Benezra R. Mad2 is a critical mediator of the chromosome instability observed upon Rb and p53 pathway inhibition. *Cancer Cell* 2011; **19**: 701–714.
26 Manning AL, Longworth MS, Dyson NJ. Loss of pRB causes centromere dysfunction and chromosomal instability. *Genes Dev* 2010; **24**: 1364–1376.
27 Mitra AK, Davis DA, Tomar S, Roy L, Gurler H, Xie J *et al.* In vivo tumor growth of high-grade serous ovarian cancer cell lines. *Gynecol Oncol* 2015; **138**: 372–377.
28 Fry DW, Harvey PJ, Keller PR, Elliott WL, Meade M, Trachet E *et al.* Specific inhibition of cyclin-dependent kinase 4/6 by PD 0332991 and associated antitumor activity in human tumor xenografts. *Mol Cancer Ther* 2004; **3**: 1427–1438.
29 Dean JL, Thangavel C, McClendon AK, Reed CA, Knudsen ES. Therapeutic CDK4/6 inhibition in breast cancer: key mechanisms of response and failure. *Oncogene* 2010; **29**: 4018–4032.
30 Konecny GE, Winterhoff B, Kolarova T, Qi J, Manivong K, Dering J *et al.* Expression of p16 and retinoblastoma determines response to CDK4/6 inhibition in ovarian cancer. *Clin Cancer Res* 2011; **17**: 1591–1602.
31 Michaud K, Solomon DA, Oermann E, Kim J-S, Zhong W-Z, Prados MD *et al.* Pharmacologic inhibition of cyclin-dependent kinases 4 and 6 arrests the growth of glioblastoma multiforme intracranial xenografts. *Cancer Res* 2010; **70**: 3228–3238.
32 Ngan VK, Bellman K, Hill BT, Wilson L, Jordan MA. Mechanism of mitotic block and inhibition of cell proliferation by the semisynthetic Vinca alkaloids vinorelbine and its newer derivative vinflunine. *Mol Pharmacol* 2001; **60**: 225–232.
33 Carmena M, Wheelock M, Funabiki H, Earnshaw WC. The chromosomal passenger complex (CPC): from easy rider to the godfather of mitosis. *Nat Rev Mol Cell Biol* 2012; **13**: 789–803.
34 Hirota T, Lipp JJ, Toh B-H, Peters J-M. Histone H3 serine 10 phosphorylation by Aurora B causes HP1 dissociation from heterochromatin. *Nature* 2005; **438**: 1176–1180.
35 van der Horst A, Lens SMA. Cell division: control of the chromosomal passenger complex in time and space. *Chromosoma* 2014; **123**: 25–42.
36 Sugiyama K, Sugiura K, Hara T, Sugimoto K, Shima H, Honda K *et al.* Aurora-B associated protein phosphatases as negative regulators of kinase activation. *Oncogene* 2002; **21**: 3103–3111.
37 Leber B, Maier B, Fuchs F, Chi J, Riffel P, Anderhub S *et al.* Proteins required for centrosome clustering in cancer cells. *Sci Transl Med* 2010; **2**: 33ra38.
38 Liedtke S, Stephan M, Kögler G. Oct4 expression revisited: potential pitfalls for data misinterpretation in stem cell research. *Biol Chem* 2008; **389**: 845–850.
39 Cancer Genome Atlas Research Network, Integrated genomic analyses of ovarian carcinoma. *Nature* 2011; **474**: 609–615.
40 Weinberg RA. The retinoblastoma protein and cell cycle control. *Cell* 1995; **81**: 323–330.
41 Yu JJ, Zhou LD, Zhao TT, Bai W, Zhou J, Zhang W. Knockdown of Aurora-B inhibits the growth of non-small cell lung cancer A549 cells. *Oncol Lett* 2015; **10**: 1642–1648.
42 Wilkinson RW, Odedra R, Heaton SP, Wedge SR, Keen NJ, Crafter C *et al.* AZD1152, a selective inhibitor of Aurora B kinase, inhibits human tumor xenograft growth by inducing apoptosis. *Clin Cancer Res* 2007; **13**: 3682–3688.
43 Kim H-J, Cho JH, Quan H, Kim J-R. Down-regulation of Aurora B kinase induces cellular senescence in human fibroblasts and endothelial cells through a p53-dependent pathway. *FEBS Lett* 2011; **585**: 3569–3576.
44 Chicas A, Wang X, Zhang C, McCurrach M, Zhao Z, Mert O *et al.* Dissecting the unique role of the retinoblastoma tumor suppressor during cellular senescence. *Cancer Cell* 2010; **17**: 376–387.
45 Lieman JH, Worley LA, Harbour JW. Loss of Rb-E2F repression results in caspase-8-mediated apoptosis through inactivation of focal adhesion kinase. *J Biol Chem* 2005; **280**: 10484–10490.
46 Rizzo S, Hersey JM, Mellor P, Dai W, Santos-Silva A, Liber D *et al.* Ovarian cancer stem cell-like side populations are enriched following chemotherapy and overexpress EZH2. *Mol Cancer Ther* 2011; **10**: 325–335.
47 Desjardins M, Xie J, Gurler H, Muralidhar GG, Sacks JD, Burdette JE *et al.* Versican regulates metastasis of epithelial ovarian carcinoma cells and spheroids. *J Ovarian Res* 2014; **7**: 70.
48 Klijn C, Durinck S, Stawiski EW, Haverty PM, Jiang Z, Liu H *et al.* A comprehensive transcriptional portrait of human cancer cell lines. *Nat Biotechnol* 2014; **33**: 306–312.